Journal of Materials Chemistry B

ROYAL SOCIETY OF CHEMISTRY

PAPER

View Article Online
View Journal | View Issue

Cite this: J. Mater. Chem. B, 2023, 11, 6075

Electrochemical detection of cholesterol in human biofluid using microneedle sensor

Zhanhong Li, †[ab] Sachin Kadian,†[c] Rupesh K. Mishra,*[de] Tiangang Huang,[b] Chen Zhou,[a] Shuyuan Liu,[a] Zifeng Wang,[a] Roger Narayan *[cf] and Zhigang Zhu *[ab]

The development of a straightforward, economical, portable, and highly sensitive sensing platform for the rapid detection of cholesterol is desirable for the early diagnosis of several pathologic conditions. In this work, we present a fascinating skin-worn microneedle sensor for monitoring cholesterol in interstitial fluid samples. The microneedle sensor was developed by incorporating platinum (Pt) and silver (Ag) wires within pyramidal microneedles containing a microcavity opening; cholesterol oxidase (ChOx) was coupled on the Pt transducer surface using bovine serum albumin and Nafion. Under optimal conditions, the enzymatic microneedle sensor exhibited high sensitivity (0.201 μA μM^{-1}) towards cholesterol in buffer solution, with good linearity over the 1–20 μM range and a correlation coefficient of 0.9910. The analytical performance of the microneedle sensor was also investigated in artificial interstitial fluid and a skin-mimicking phantom gel; the sensor showed great potential for skin-worn/wearable applications with excellent linearity and a low detection limit. In addition, the developed microneedle sensor showed satisfactory stability and good selectivity towards cholesterol in the presence of potential interfering biomolecules, including glucose, lactic acid, uric acid, and ascorbic acid. This sensor exhibits enormous promise for straightforward, sensitive, and minimally invasive monitoring of cholesterol.

Received 8th October 2022,
Accepted 22nd May 2023

DOI: 10.1039/d2tb02142k

rsc.li/materials-b

1. Introduction

Cholesterol ((3b)-cholest-5-en-3-ol) is an organic biomolecule that forms an integral structural component of cell membranes.[1–3] In addition, cholesterol plays a significant role in the biosynthesis of vitamin D, steroid hormones, and bile acid, which aids in lipid digestion.[2] An increased or decreased level of cholesterol with respect to the normal range (2.83–5.20 mM) is associated with various pathologic conditions.[4–7] For instance, a low cholesterol level is associated with malnutrition, sepsis, low lipoprotein levels, cerebral hemorrhage, anemia, and cancer; a high cholesterol level is associated with coronary heart disease, cerebral thrombosis, hypertension, myocardial infarction, stroke, and atherosclerosis.[5,8–14] The development of a sensitive, straightforward-to-use, accurate, and selective sensing platform for the continuous monitoring of cholesterol levels can facilitate the early diagnosis of the abovementioned cardiovascular and neurological conditions.

The existing conventional techniques used for the determination of cholesterol include spectrophotometry, colorimetry, high-performance liquid chromatography, electrochemiluminescence, fluorescence,[15–17] and electrochemistry.[18–22] Although these techniques exhibit good sensitivity towards cholesterol, their limitations include high cost, time consumption, poor specificity, and difficult standardization; additional shortcomings include the use of sophisticated instrumentation, the requirement of experienced operators, and the requirement of sample preprocessing.[23,24] Due to several interesting characteristics such as high specificity, high simplicity, high sensitivity, and low cost, the development of electrochemical sensors for *in vitro* monitoring of cholesterol has gained significant attention from both academia as well as the pharmaceutical industry.[25,26] For instance, Ghanei *et al.* (2019) developed an electrochemical sensor using gold and titanium dioxide nanoparticle-modified multiwall carbon nanotubes for cholesterol detection.[27] Mahdi *et al.* described the use of copper

[a] School of Medical Instrument and Food Engineering, University of Shanghai for Science and Technology, Shanghai, 200093, China. E-mail: zgzhu@usst.edu.cn
[b] School of Environmental and Materials Engineering, Shanghai Polytechnic University, 2360 Jinhai Road, Shanghai, 201209, China
[c] Joint Department of Biomedical Engineering, University of North Carolina and North Carolina State University, Raleigh, NC 27695, USA
[d] IdentifySensors Biologics, 1203 W. State Street, West Lafayette, IN 47907, USA
[e] School of Materials Engineering, Purdue University, 701 West Stadium Avenue, West Lafayette, IN 47907, USA
[f] Department of Materials Science and Engineering, North Carolina State University, Raleigh, NC 27695, USA. E-mail: rjnaraya@ncsu.edu
† Authors contributed equally to this work.

nanoparticles and an indole-modified pencil graphite electrode-based electrochemical sensor for the determination of cholesterol; a lowest limit of detection 4.98 nM was demonstrated using this approach.[28] Yulizara *et al.* developed a molybdenum disulfide- and nickel oxide-decorated screen-printed carbon electrode for cholesterol detection.[29] The sensor exhibited good sensitivity, with a limit of detection of 0.24 mg dL^{-1}. Similarly, Thakur *et al.* fabricated a NiVP/Pi coated Whatman filter paper-based flexible sensing probe for cholesterol detection in serum samples.[30] Despite the significant progress in electrochemical biosensors, these approaches rely on the use of nanomaterial-based electrode surface modification processes and remain unable to continuously monitor the cholesterol level in physiologically relevant fluids.[31–37] The development of a wearable electrochemical sensing platform that can address the abovementioned issues by continuously monitoring the cholesterol level in interstitial fluid with high specificity is highly desirable.

Wearable sensor technology has proliferated in recent years, providing enormous opportunities for the development of personalized medical devices.[38] Among the various recently developed wearable sensors, microneedle-based sensors have gained significant attention for rapid, facile, minimally invasive, and continuous transdermal sensing of several biomolecules in the interstitial fluid.[38–42] Microneedles are low-cost micrometer-size devices that are capable of creating artificial pores in the skin by disrupting the outermost stratum corneum layer of the epidermis, enabling access to interstitial fluid with minimal pain and damage.[43–45] Microneedle arrays have also been used for real-time monitoring of biomarkers such as alcohol, lactate, glucose, organophosphate, L-dopa, and potassium ions.[38,39,44,45] To the best of our knowledge, no prior study has been reported for the development of microneedles for the continuous monitoring of cholesterol in interstitial fluid to this point.

In this study, we have evaluated a novel biocatalytic microneedle sensor for continuous and minimally invasive monitoring of cholesterol in interstitial fluid samples. The three-electrode system containing the working, counter, and reference electrodes was developed by integrating Pt and Ag wires within a hollow microneedle array. As shown in Fig. 1, cholesterol oxidase (ChOx)-based biocatalytic detection of cholesterol was performed at the ChOx coupled Pt wire infused microneedle electrode through chronoamperometric measurements of hydrogen peroxide (H_2O_2). Upon optimization, the developed microneedle sensor offered high sensitivity towards cholesterol along with a linear current response and favorable stability. Further, the as-prepared sensor also exhibited excellent selectivity in the presence of potential interfering biomolecules, including glucose, lactic acid, uric acid, and ascorbic acid. Moreover, for the proof-of-concept, the analytical performance and wearable application potential of the microneedle sensor array were examined in artificial interstitial fluid and a skin-mimicking phantom gel model. The obtained results suggest that a microneedle sensor can also be used for the development of on-body electrochemical devices for the detection of other biomarkers in interstitial fluid.

2. Experimental methods

2.1. Chemicals and reagents

Enzyme cholesterol oxidase (from *Streptomyces* sp., ≥20 units per mg protein, lyophilized powder), cholesterol (≥99%), agarose, Nafion (5 wt% in a mixture of water and lower aliphatic alcohols, contains 45% water), and albumin from bovine serum

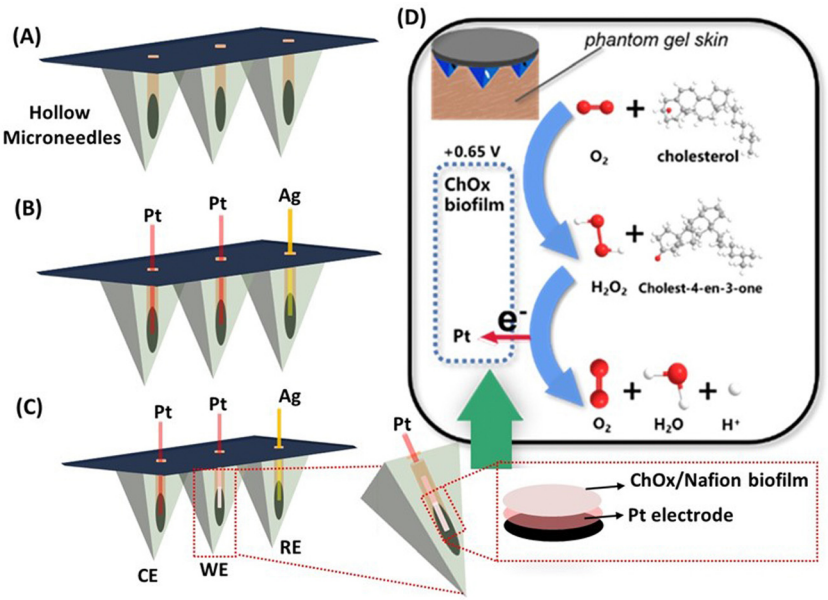

Fig. 1 Schematic illustration of (A) the hollow microneedle, (B) Pt and Ag wires integrated with the microneedle array, (C) ChOx/Nafion functionalization of the Pt electrode, and (D) the reaction mechanism associated with the minimally invasive wearable microneedle sensor for the detection of cholesterol.

(lyophilized powder, ≥98%) were purchased from a commercial source (Sigma Aldrich China Inc., Shanghai, China). Acetaminophen, ascorbic acid, uric acid, potassium chloride, sodium chloride, potassium phosphate monobasic (KH_2PO_4), potassium phosphate dibasic (K_2HPO_4), and ethyl alcohol were obtained from Sinopharm Chemical Reagent Co. Ltd. (Shanghai, China). All of the stock solutions and dilutions used in the experiments were prepared in fresh deionized (DI) water that was obtained from a Milli-Q system (18.2 MΩ cm at 25 °C).

2.2. Instrumentations, methods, and microneedle sensor fabrication

A CHI760e electrochemical workstation with a three-electrode system (CHI Instruments Inc., Shanghai, China) connected to a personal computer was used for all of the electrochemical analysis activities. All of the chronoamperometric experiments were performed in a 0.1 M phosphate buffer solution (PBS) (pH 7.4) and artificial interstitial fluid. The stock solution of cholesterol was prepared in PBS solution containing 10% Triton X-100. The pH value of the PBS solution was adjusted by balancing the ratio of monobasic and dibasic sodium phosphate; 0.5% NaCl was added to increase the conductivity of the solution.

The hollow microneedle array was fabricated through our previously reported procedure using Solidworks (Dassault Systemes S.A., Velizy, France) computer models.[39,46] The structure of the substrate was designed Magics RP 13 (Materialise NV, Leuven, Belgium). Each pyramidal shape microneedle with a triangular base exhibited a height of 1500 μm, an edge length of 1250 μm, and a vertical cylindrical hole with a diameter of 425 μm. The vertical hole in each needle was located on one face of the pyramid structure. In the structure, each microneedle was placed 1 mm apart from each other. Further, the vertical cylindrical bore in the microneedle array enables a stable enzymatic sensing platform to be constructed without disturbing its skin penetration potential. The three-electrode system, with working, counter and reference electrodes, was prepared by inserting Pt and Ag wires into the vertical cylindrical holes that were located in the microneedles. To construct the enzymatic electrochemical transducer, the ChOx solution was prepared by suspending 5 mg of enzyme lyophilized powder in 200 μL of 0.1 M PBS (pH 7.4) along with 5 mg bovine serum albumin to enhance the enzymatic stability. Next, 1% Nafion solution was prepared by diluting 5% Nafion stock solution in ethanol. Afterward, the ChOx/Nafion mixture was prepared by mixing the above-prepared fresh ChOx solution into 1% Nafion at a volume ratio of 3 : 7. Subsequently, 3 μL of the ChOx/Nafion mixture was drop-casted onto the Pt wire integrated microneedle working electrode and allowed to dry under ambient conditions for 2 h. The 1% Nafion was used to prevent enzyme dripping.

2.3. *In vitro* detection of cholesterol

The analytical performance of the as-developed microneedle sensor towards cholesterol was initially investigated *in vitro* in freshly prepared PBS electrolyte solution (0.1 M, pH 7.4). Different cholesterol concentrations were prepared by diluting the stock solution in 0.1 M PBS solution; these solutions were used to evaluate the detection range and selectivity through chronoamperometric measurements. The chronoamperometric response against electrochemical oxidation or reduction of the peroxide product for different concentrations of cholesterol was recorded at a fixed potential of +0.65 V for 60 s. The selectivity of the as-prepared microneedle sensor was examined in the presence of potential interferents, including glucose, lactic acid, uric acid, and ascorbic acid. The artificial interstitial fluid was prepared according to the method reported by Fogh-Andersen *et al.*[47]

2.4. Preparation of human skin-mimicking phantom gel

To investigate the use of the microneedle sensor for wearable applications, a skin-mimicking phantom gel was prepared using a procedure that was reported in recently published work.[39,48] In brief, 140 mg of agarose was dissolved in 10 mL of PBS solution (1.4%) and kept at 120 °C under constant stirring until complete dissolution. Afterward, the as-prepared homogenous agarose mixture was subjected to solidification inside a Petri dish. Next, five different concentrations (2–10 μM) of cholesterol were dispensed into five different Petri dishes and permitted to diffuse into the gel for 60 minutes at room temperature. For skin-mimicking phantom gel experiments, the as-developed microneedle sensor was examined in the cholesterol-diffused phantom gel after 1 minute of contact between the needle tips and the gel; the detection of cholesterol utilized amperometric analysis.

3. Results and discussion

3.1. Design and principle of wearable microneedle sensor

The minimally invasive wearable microneedle sensor was fabricated by integrating Ag and Pt wires (100 μm diameter) within an array of sharp microneedles (Fig. 1A) that contain microcavities. Among three different microneedle electrodes, one of the Pt wire-infused microneedle electrodes (Fig. 1B) was used as a counter electrode. Another Pt wire-infused microneedle electrode functionalized with a ChOx/Nafion mixture was used as a working electrode (Fig. 1C). An Ag wire integrated microneedle electrode served as a reference electrode. The three-electrode electrochemical sensor relied on the catalysis of cholesterol driven by ChOx in the presence of oxygen and the production of H_2O_2. Pt is a well-known catalyst that has a strong catalytic activity for peroxide electrooxidation; the H_2O_2 generated by ChOx catalyzed oxidation of cholesterol was detected and correlated with the target cholesterol concentration by recording the chronoamperometric response through the Pt electrode at an applied anodic potential (+0.65 V).

A schematic illustration of the existing biocatalytic reaction of cholesterol through the immobilized ChOx enzyme on the working electrode is shown in Fig. 1D. It should be noted that 1% Nafion mixed with ChOx was used to prevent enzyme dripping. Further, the analytical performance of as-prepared

enzymatic microneedle sensors was systematically investigated in different environments, including PBS solution (pH 7.4), artificial interstitial fluid, and a skin-mimicking phantom gel.

3.2. Morphological characteization of microneedles

Before utilizing the as-prepared hollow microneedle array for the development of minimally invasive wearable microneedle sensor, imaging was performed to confirm the structure of the microneedle array. Fig. 2 displays scanning electron microscopy (SEM) images of a hollow microneedle array. It can be observed from the Fig. 2A that each pyramidal shaped microneedle contains a triangular base and a vertical cylindrical hole (Fig. 2B) with a diameter of 425 μm.

3.3. Analytical performance of microneedle sensor in buffer solution

Wearable microneedle sensors are becoming an important tool for the biosensing of human body fluids. However, their efficacy and significance are highly dependent on the ease of operation and precision of the devices. Therefore, the analytical performance and efficacy of the as-developed platinum-based wearable microneedle sensor were first examined by detecting different concentrations (1–20 μM) of cholesterol in 0.1 M PBS solution (pH 7.4). The analytical response of the enzymatic sensor towards cholesterol was measured by recording chronoamperometric responses. The current was sampled for 100 s at an applied potential of 0.65 V (*vs.* Ag/AgCl) reference electrode. Fig. 3(A) demonstrates the chronoamperometric response of the microneedle sensor at an applied potential of 0.65 V with various concentrations of cholesterol (1–20 μM) in 0.1 M PBS solution. It can be observed from Fig. 3(A) that the enzymatic sensor exhibited a well-defined amperometric response against increasing concentration of cholesterol (1–20 μM) without any change in the shape of chronoamperograms. The corresponding calibration plot between obtained current and cholesterol concentrations was shown in Fig. 3B, signifying a highly linear response throughout the tested cholesterol concentrations with a sensitivity of 0.201 μA μM^{-1} and a correlation coefficient of 0.9910. All the cholesterol concentrations were tested in triplicate and repeated several times (n = 5). These results suggest that the microneedle sensor was capable of detecting cholesterol over a dynamic range with high affinity and sensitivity.

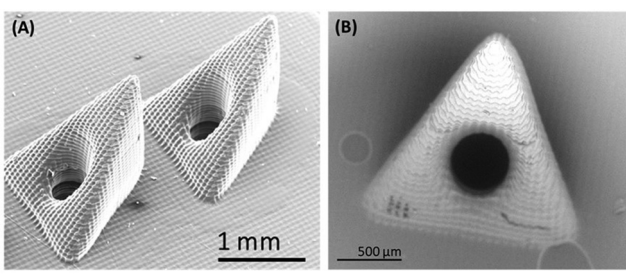

Fig. 2 Illustration of SEM image of (A) hollow microneedle array and (B) single hollow microneedle.

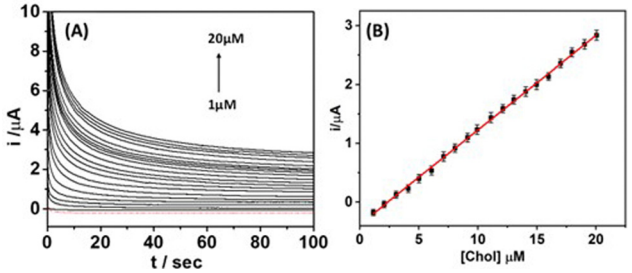

Fig. 3 (A) Chronoamperometric response of the microneedle sensor toward increasing concentrations of cholesterol (1 μM increments) in PBS solution over a 1–20 μM range; the potential was applied at +0.65 V (*vs.* Ag/AgCl). (B) The respective calibration plots for up to 20 μM cholesterol based on sampling the current at 100 s.

3.4. Cholesterol detection in artificial interstitial fluid

Since the long-term exposure of the biosensor to a complicated medium may affect the analytical response, it is important to assess the performance of the microneedle sensor in artificial interstitial fluid. The microneedle sensor was covered with 100 μL of artificial interstitial fluid; a baseline was recorded by scanning the current for 100 s using an amperometric scan (+0.65 V *vs.* Ag/AgCl) until the overlapping of the last two scans. Fig. 4A represents the chronoamperometric response of the microneedle sensor at an applied potential of 0.65 V for various concentrations of cholesterol (1–15 μM) in artificial interstitial fluid. It was noted that the microneedle sensor displayed an obvious, uninterrupted, and noise-free distinctive amperometric response for each tested concentration of cholesterol. The resulting calibration plot (Fig. 4B) between the obtained current and cholesterol concentrations exhibited high linearity, with a correlation coefficient of 0.9990 and a lower detection limit as low as 0.5 μM (estimated through the standard equation: LOD = 3.3 σ/m, where σ is the standard error of the blank samples and m is the slope of the calibration curve). Further, a control experiment was also carried out without using the ChOx enzyme on the Pt electrode surface. The obtained results (data not shown) indicated no significant changes in the amperometric response upon increasing the cholesterol concentration (similar to those observed for the blank buffer solution). These

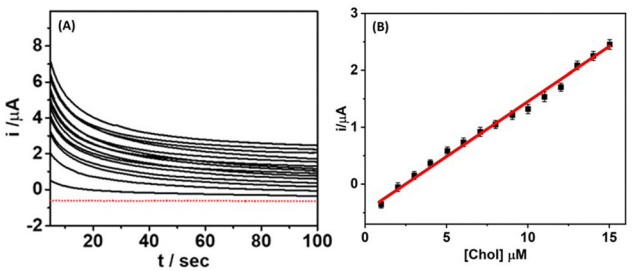

Fig. 4 (A) Chronoamperometric response of the microneedle sensor toward increasing concentrations of cholesterol (1 μM increments) in an artificial interstitial fluid sample over the 1–15 μM range; potential applied at +0.65 V (*vs.* Ag/AgCl). (B) The respective calibration plots up to 15 μM cholesterol based on sampling the current at 100 s.

results further indicate the successful operation of the microneedle sensor for the analysis of interstitial fluid.

3.5. Cholesterol detection in skin-mimicking phantom gel

The analytical performance of the microneedle sensor was evaluated by performing cholesterol detection in a skin-mimicking phantom gel model. An agarose gel human skin model (Fig. 5A) diffused with different cholesterol concentrations (2–10 μM) was used for cholesterol detection. Fig. 5B demonstrates the chronoamperometric response of the microneedle sensor at an applied potential of 0.65 V for various concentrations of cholesterol (2–10 μM) in the skin-mimicking phantom gel. It was observed that the microneedle sensor exhibited a well-defined amperometric response for each diffused concentration of cholesterol in the skin-mimicking phantom gel. Based on the obtained chronoamperometric response, a calibration curve (Fig. 5C) among obtained current and cholesterol concentrations was plotted, which demonstrated a highly linear dynamic range between 2–10 μM with a correlation coefficient of 0.9996. This unique analytical performance of the microneedle sensor in a skin-mimicking model suggests that this type of sensor can potentially be used for on-body cholesterol detection. In addition, this experiment shows that the microneedle sensor contains a stable enzymatic layer, which is not affected by the phantom gel penetration process.

The microcavity within the microneedle helps protect the immobilized enzyme (ChOx) layer during skin penetration and allows access to interstitial fluid. Also, this skin-mimicking model assessment confirmed that the microneedle sensor shows similar sensitivity to that observed during the above-mentioned *in vitro* studies. The microneedle tips were found to be sharp enough to allow penetration into the skin-mimicking phantom gel by applying gentle pressure. The microneedle array was noted to retain its mechanical properties and morphology after multiple penetrations into the skin-mimicking phantom gel.

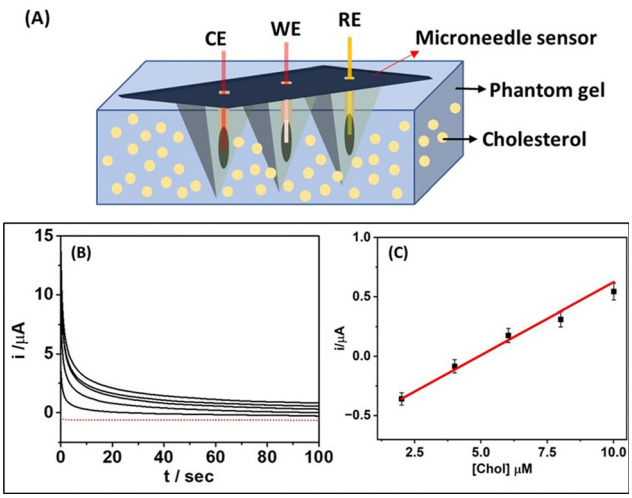

Fig. 5 (A) Schematic illustration of microneedle sensor-based detection of cholesterol in skin-mimicking phantom gel. (B) Chronoamperometric response of microneedle sensor toward increasing concentrations of cholesterol (2 μM increments) in the skin-mimicking phantom gel over the 2–10 μM range; potential applied at +0.65 V (*vs.* Ag/AgCl). (C) The corresponding current response plots up to 10 μM cholesterol based on sampling the current at 100 s.

3.6. Selectivity, reproducibility and stability assay

Since selectivity is also a critical parameter for evaluating the efficacy and clinical application potential of a biosensor,[38,43,54] the selectivity of the microneedle sensor was investigated by recording the chronoamperometric response in the presence of potential interferents such as glucose (Glu, 500 μM), lactic acid (LA, 250 μM), uric acid (UA, 250 μM) and ascorbic acid (AA, 250 μM) along with a concentration of cholesterol (10 μM). In this study, a standard concentration of these interferents was used separately and added to the sensing electrode surface. Fig. 6A displays the analytical response of the microneedle sensor in the presence of the abovementioned interferents; a negligible response was obtained when ascorbic acid, uric acid, lactic acid, and glucose were tested. This minimal response to the interferents was attributed to the presence of the selectivity of the ChOx enzyme on the surface of the working electrode. In addition, a control experiment was conducted on the microneedle sensor by eliminating the adhesion of ChOx enzyme and the other necessary bioreagent layer. Upon the addition of cholesterol of different concentrations to the sensing electrode surface, no significant changes in the oxidation/reduction current were recorded. These selectivity assay results indicate the ability of the microneedle sensor for robust and selective detection of cholesterol. In addition, the reproducibility of the microneedle sensor was evaluated by fabricating multiple biosensing devices under similar processing conditions; the response characteristics were observed to be comparable with an RSD of 2.05%. Next, the long-term stability of developed microneedle sensor was determined by analyzing the variation in sensing response at regular 7 days interval for four weeks and shown in Fig. 6B. The developed microneedle sensor was kept at 4 °C when it was not in use. It was observed that the sensor retained 86% of sensing response even after four weeks of storage, which confirms the practicability of the developed microneedle sensor. Additionally, a comparison (Table 1) of the analytical performance of our proposed microneedle sensor and previously reported methods suggested that when considered together, all parameters such as sensor type, linearity

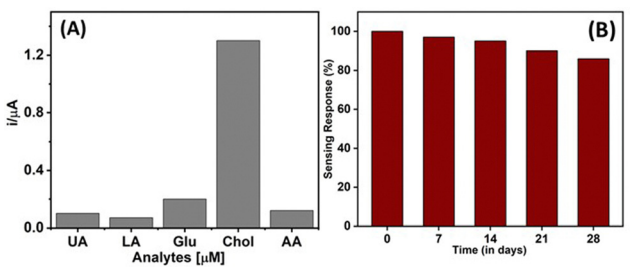

Fig. 6 (A) Selectivity of the microneedle sensor in the presence of potential interferents and (B) long-term stability of the microneedle sensor.

Table 1 Comparison of the analytical performance of our proposed sensor with previous reports

Sensor type	Materials used	Linear range	R^2	LOD (μM)	Methodology	Ref.
Paper-based	ChOx/G/PVP/PANI	0.05–10 mM	0.999	1	Complex	49
Hydrogels-based	PANI-Pt NPs/GCE	0.3–9 mM	0.997	300	Simple	50
Glassy carbon based	ChOx/Nano-Pt/MWCNT-PANI	0.002–0.5 mM	0.993	0.8	Complex	51
FET-based	ChOx/PANI/ZnO	0.5–16.6 mM	0.998	250	Complex	52
Microneedle array based	ChOx/Pt NPs/PANI/MEA	1–12 mM	0.992	440	Complex	53
3D printed microneedle based	ChOx/Pt wire	1–20 μM	0.996	0.5	Simple	This work

range, material used, limit of detection limit, methodology, and R^2 value, the proposed sensing platform showed superiority over many previously published approaches and equivalence to the best-performing ones.

4. Conclusions

In this work, we have demonstrated the design and analytical performance of an enzymatic (ChOx) microneedle sensor for minimally invasive continuous monitoring of cholesterol in real human biofluid. The detection method depends on independent electrochemical measurements involving biocatalytic and redox processes. The microneedle sensor relies on the catalysis of cholesterol driven by ChOx in the presence of oxygen and the production of H_2O_2, which was measured by a chronoamperometric technique at an applied potential of +0.65 V. The microneedle sensor exhibited an excellent analytical signature and performance towards cholesterol in artificial interstitial fluid as well as a skin-mimicking phantom gel model with high sensitivity, good stability, a wide detection range, and excellent selectivity in the presence of potential interferents. The results suggest that the wearable microneedle sensor can also be used for the development of on-body electrochemical detection of other biomarkers present in the interstitial fluid. Future efforts are focused on integrating electronic instrumentation along with wireless communication and signal processing functionalities on the microneedle sensor and investigating the potential of the resulting wearable transdermal microneedle sensor device for real-time remote monitoring of cholesterol levels.

Conflicts of interest

There are no conflicts to declare.

Acknowledgements

This work was supported by the University Capacity Building Project of the Shanghai Science and Technology Commission (21010502800). Authors would like to acknowledge Roger Sachan (Department of Materials Science and Engineering, NC State University, Raleigh, NC, USA), Pratik Joshi (Department of Materials Science and Engineering, NC State University, Raleigh, NC, USA) and Sina Azizi Machekposhti (Joint Department of Biomedical Engineering, NC State University, Raleigh, NC, USA) for their help in designing, collecting SEM image and manufacturing the microneedles, respectively.

References

1 M. M. Rahman and A. M. Asiri, *Talanta*, 2015, **140**, 96–101.
2 N. Batra, M. Tomar and V. Gupta, *Biosens. Bioelectron.*, 2015, **67**, 263–271.
3 M. B. Gholivand and M. Khodadadian, *Biosens. Bioelectron.*, 2014, **53**, 472–478.
4 H. J. Harwood, C. E. Chandler, L. D. Pellarin, F. W. Bangerter, R. W. Wilkins, C. A. Long, P. G. Cosgrove, M. R. Malinow, C. A. Marzetta and J. L. Pettini, *J. Lipid Res.*, 1993, **34**(3), 377–395.
5 D. Sharma, J. Lee, J. Seo and H. Shin, *Sensors*, 2017, **17**(9), 2128.
6 G. A. Tlğ, D. K. Zeybek and S. Pekyardlmcl, *Chem. Pap.*, 2016, **70**(6), 695–705.
7 S. D. de Ferranti, A. M. Rodday, S. K. Parsons, W. L. Cull, K. G. O'Connor, S. R. Daniels and L. K. Leslie, *J. Pediatr.*, 2017, **185**, 99–105.
8 J. Wang, G. J. Tan, L. N. Han, Y. Y. Bai, M. He and H. bin Liu, *J. Geriatr. Cardiol.*, 2017, 14.
9 A. Rosiek and K. Leksowski, *Ther. Clin. Risk Manage.*, 2016, 12.
10 P. Joshi, S. Shukla, S. Gupta, P. R. Riley, J. Narayan and R. Narayan, *ACS Appl. Mater. Interfaces*, 2022, **14**(32), 37149–37160.
11 P. C. Pandey, H. P. Yadav, S. Shukla and R. J. Narayan, *Chemosensors*, 2021, **9**(9), 253.
12 P. C. Pandey, S. Shukla, S. A. Skoog, R. D. Boehm and R. J. Narayan, *Sensors*, 2019, 19.
13 S. Shukla, P. Joshi, P. Riley and R. J. Narayan, *Biosens. Bioelectron.*, 2022, **216**, 114592.
14 P. C. Pandey, M. D. Mitra, S. Shukla and R. J. Narayan, *Biosensors*, 2021, **11**(4), 122.
15 S. Kadian and G. Manik, *Food Chem.*, 2020, **317**, 126457.
16 S. Kadian and G. Manik, *Luminescence*, 2020, **35**(5), 763–772.
17 S. Kadian, S. K. Sethi and G. Manik, *Mater. Chem. Front.*, 2021, **5**(2), 627–658.
18 Y. Zhang, Y. N. Wang, X. T. Sun, L. Chen and Z. R. Xu, *Sens. Actuators, B*, 2017, **246**, 118–126.
19 H. Y. Hsieh, L. H. Li, R. Y. Hsu, W. F. Kao, Y. C. Huang and C. C. Hsu, *Anal. Chem.*, 2017, **89**(11), 6146–6152.
20 D. Lütjohann, I. Björkhem, S. Friedrichs, A. Kerksiek, A. Lövgren-Sandblom, W. J. Geilenkeuser, R. Ahrends,

I. Andrade, D. Ansorena, I. Astiasarán, L. Baila-Rueda, B. Barriuso, S. Becker, L. Bretillon, R. W. Browne, C. Caccia, U. Ceglarek, A. Cenarro, P. J. Crick, G. Fauler, G. Garcia-Llatas, R. Gray, W. J. Griffiths, H. Gylling, S. Harding, C. Helmschrodt, L. Iuliano, H. G. Janssen, P. Jones, L. Kaipiainen, F. Kannenberg, M. J. Lagarda, V. Leoni, A. M. Lottenberg, D. S. MacKay, S. Matysik, J. McDonald, M. Menendez-Carreño, S. B. Myrie, V. Sutti Nunes, R. E. Ostlund, E. Polisecki, F. Ramos, T. C. Rideout, E. J. Schaefer, G. Schmitz, Y. Wang, C. Zerbinati, U. Diczfalusy and H. F. Schött, *J. Steroid Biochem. Mol. Biol.*, 2019, **190**, 115–125.

21 X. Jiang, Z. Tan, L. Lin, J. He, C. He, B. D. Thackray, Y. Zhang and J. Ye, *Small Methods*, 2018, **2**(11), 1800182.

22 P. Wei, Z. Zhu, R. Song, Z. Li and C. Chen, *Electrochim. Acta*, 2019, **317**, 93–101.

23 A. Wisitsoraat, P. Sritongkham, C. Karuwan, D. Phokharatkul, T. Maturos and A. Tuantranont, *Biosens. Bioelectron.*, 2010, **26**(4), 1514–1520.

24 K. V. Mokwebo, O. S. Oluwafemi and O. A. Arotiba, *Sensors*, 2018, **18**(10), 3368.

25 Z. H. Li, X. L. Zhao, R. M. Song, C. Chen, P. J. Wei and Z. G. Zhu, *Chem. Phys. Lett.*, 2018, **712**, 71–77.

26 Z. H. Li, X. L. Zhao, X. C. Jiang, Y. H. Wu, C. Chen, Z. G. Zhu, J. L. Marty and Q. S. Chen, *Electroanalysis*, 2018, **30**(8), 1811–1819.

27 D. G. Kariz, E. Darabi and S. M. Elahi, *Nano Lett.*, 2022, **12**(1), 113–123.

28 M. Shahriarinour, F. Rahimi, R. Elham Siahbani, Kochakinejad and S. Kaki, *J. Iran. Chem. Soc.*, 2022, **19**(1), 159–171.

29 H. A. Ariyanta, T. A. Ivandini and Y. Yulizar, *FlatChem*, 2021, **29**, 100285.

30 N. Thakur, D. Mandal and T. C. Nagaiah, *Chem. Commun.*, 2022, **58**, 2706.

31 N. Soda and O. A. Arotiba, *Bioelectrochemistry*, 2017, **118**, 14–18.

32 M. Chatterjee, P. Nath, S. Kadian, A. Kumar, V. Kumar, P. Roy, G. Manik and S. Satapathi, *Sci. Rep.*, 2022, **12**(1), 9061.

33 S. Kadian, G. Manik, N. Das, P. Nehra, R. P. Chauhan and P. Roy, *J. Mater. Chem. B*, 2020, **8**(15), 3028–3037.

34 S. Kadian, N. Chaulagain, H. Rajashekhar, D. Vrushabendrakumar, G. Manik and K. Shankar, in Proceedings of IEEE Sensors, 2021, vol. 2021.

35 S. Kadian, G. Manik, A. Kalkal, M. Singh and R. P. Chauhan, *Nanotechnology*, 2019, **30**(43), 435704.

36 A. Kalkal, S. Kadian, R. Pradhan, G. Manik and G. Packirisamy, *Mater. Adv.*, 2021, **2**, 5513–5541.

37 S. Kadian, G. Manik, N. Das and P. Roy, *Microchim. Acta*, 2020, **187**, 1–10.

38 A. M. V. Mohan, J. R. Windmiller, R. K. Mishra and J. Wang, *Biosens. Bioelectron.*, 2017, **91**, 574–579.

39 K. Y. Goud, C. Moonla, R. K. Mishra, C. Yu, R. Narayan, I. Litvan and J. Wang, *ACS Sens.*, 2019, **4**(8), 2196–2204.

40 U. Heredia-Rivera, V. Kasi, A. Krishnakumar, S. Kadian, A. K. Barui, Z. He, H. Wang, L. Stanciu and R. Rahimi, *ACS Appl. Mater. Interfaces*, 2023, **15**, 17078–17090.

41 M. Singh, S. Kadian and G. Manik, Polymers in Adhesive Applications, in *Encyclopedia of Materials: Plastics and Polymers*, ed. M.S.J. Hashmi, Elsevier, 2022, 370–381, DOI: **10.1016/B978-0-12-820352-1.00124-3**.

42 A. Krishnakumar, S. Kadian, U. Heredia Rivera, S. Chittiboyina, S. A. Lelièvre and R. Rahimi, *ACS Biomater. Sci. Eng.*, 2023, **9**(3), 1620–1628.

43 R. K. Mishra, K. Y. Goud, Z. Li, C. Moonla, M. A. Mohamed, F. Tehrani, H. Teymourian and J. Wang, *J. Am. Chem. Soc.*, 2020, **142**(13), 5991–5995.

44 H. Teymourian, F. Tehrani, K. Mahato and J. Wang, *Adv. Healthcare Mater.*, 2021, 10.

45 B. Ciui, A. Martin, R. K. Mishra, B. Brunetti, T. Nakagawa, T. J. Dawkins, M. Lyu, C. Cristea, R. Sandulescu and J. Wang, *Adv. Healthcare Mater.*, 2018, **7**(7), 1701264.

46 J. R. Windmiller, N. Zhou, M. C. Chuang, G. Valdés-Ramírez, P. Santhosh, P. R. Miller, R. Narayan and J. Wang, *Analyst*, 2011, **136**(9), 1846–1851.

47 N. Fogh-Andersen, B. M. Altura, B. T. Altura and O. Siggaard-Andersen, *Clin. Chem.*, 1995, **41**(10), 1522–1525.

48 H. Chang, M. Zheng, X. Yu, A. Than, R. Z. Seeni, R. Kang, J. Tian, D. P. Khanh, L. Liu, P. Chen and C. Xu, *Adv. Mater.*, 2017, **29**(37), 1702243.

49 N. Ruecha, R. Rangkupan, N. Rodthongkum and O. Chailapakul, *Biosens. Bioelectron.*, 2014, **52**, 13–19.

50 L. Li, Y. Wang, L. Pan, Y. Shi, W. Cheng, Y. Shi and G. Yu, *Nano Lett.*, 2015, **15**(2), 1146–1151.

51 Z. H. Xu, X. D. Cheng, J. H. Tan and X. Gan, *Biotechnol. Appl. Biochem.*, 2016, **63**(6), 757–764.

52 M. A. Barik and J. C. Dutta, *Appl. Phys. Lett.*, 2014, **105**(5), 053509.

53 J. Gao, W. Huang, Z. Chen, C. Yi and L. Jiang, *Sens. Actuators, B*, 2019, **287**, 102–110.

54 S. Kadian, B. D. Arya, S. Kumar, S. N. Sharma, R. P. Chauhan, A. Srivastava, P. Chandra and S. P. Singh, *Electroanalysis*, 2018, **30**(11), 2793–2802.